MNRAS 000, 1–8 (2019) Preprint 11 August 2021 Compiled using MNRAS LATEX style file v3.0

A model for the radio/X-ray correlation in three neutron star low-mass X-ray binaries 4U 1728-34, Aql X-1 and EXO 1745-248

Erlin Qiao [1,2]★ and B.F. Liu [1,2]

[1]Key Laboratory of Space Astronomy and Technology, National Astronomical Observatories, Chinese Academy of Sciences, Beijing 100012, China
[2]School of Astronomy and Space Sciences, University of Chinese Academy of Sciences, 19A Yuquan Road, Beijing 100049, China

arXiv:1905.05996v1 [astro-ph.HE] 15 May 2019

Accepted XXX. Received YYY; in original form ZZZ

ABSTRACT

Observationally, for neutron star low-mass X-ray binaries, so far, the correlation between the radio luminosity $L_{\rm R}$ and the X-ray luminosity $L_{\rm X}$, i.e., $L_{\rm R} \propto L_{\rm X}^{\beta}$, has been reasonably well-established only in three sources 4U 1728-34, Aql X-1 and EXO 1745-248 in their hard state. The slope β of the radio/X-ray correlation of the three sources is different, i.e., $\beta \sim 1.4$ for 4U 1728-34, $\beta \sim 0.4$ for Aql X-1, and $\beta \sim 1.6$ for EXO 1745-248. In this paper, for the first time we explain the different radio/X-ray correlation of 4U 1728-34, Aql X-1 and EXO 1745-248 with the coupled advection-dominated accretion (ADAF)-jet model respectively. We calculate the emergent spectrum of the ADAF-jet model for $L_{\rm X}$ and $L_{\rm R}$ at different $\dot{m}$ ($\dot{m} = \dot{M}/\dot{M}_{\rm Edd}$), adjusting η ($\eta \equiv \dot{M}_{\rm jet}/\dot{M}$, describing the fraction of the accreted matter in the ADAF transfered vertically forming the jet) to fit the observed radio/X-ray correlations. Then we derive a fitting formula of η as a function of $\dot{m}$ for 4U 1728-34, Aql X-1 and EXO 1745-248 respectively. If the relation between η and $\dot{m}$ can be extrapolated down to a lower value of $\dot{m}$, we find that in a wide range of $\dot{m}$, the value of η in Aql X-1 is greater than that of in 4U 1728-34 and EXO 1745-248, implying that Aql X-1 may have a relatively stronger large-scale magnetic field, which is supported by the discovery of the coherent millisecond X-ray pulsation in Aql X-1.

Key words: accretion, accretion discs – stars: neutron – black hole physics – X-rays: binaries – radio continuum:stars

1 INTRODUCTION

Low-mass X-ray binaries (LMXBs) which either contain a black hole (BH) or a neutron star (NS), accreting matter from its low-mass companion star ($\lesssim 1M_{\odot}$) are ideal natural laboratories for studying the physics of accretion and jet around a BH or a NS (e.g. Migliari & Fender 2006). According to the timing and spectral features in the X-ray band, LMXBs are generally divided into two main spectral states, i.e., the high/soft state and the low/hard state (Gilfanov 2010, for review). For BH-LMXBs, when they are in the high/soft state, the accretion flow is widely believed to be dominated by the optically thick, geometrically thin, cool accretion disc (Shakura & Sunyaev 1973), and the X-ray spectrum can be well described by a multi-color blackbody spectrum (e.g. Mitsuda et al. 1984; Makishima et al. 1986; Merloni et al. 2000). Whereas, for NS-LMXBs, besides the emission from the disc, there is a significant thermal emission from the boundary layer between the accretion disc and the surface of the NS (Popham & Narayan 1992; Inogamov & Sunyaev 1999; Popham & Sunyaev 2001; Gilfanov & Sunyaev 2014, for review). Observationally, for both BH-LMXBs and NS-LMXBs, when they are in the low/hard state, generally, the accretion flow is suggested to be dominated by the optically thin, geometrically thick, hot, advection-dominated accretion flow (ADAF) (Done et al. 2007, for review). Theoretically, the ADAF solution has been studied in detail by several researchers since it was discovered in 1970's (Ichimaru 1977; Rees et al. 1982; Narayan & Yi 1994, 1995a,b; Abramowicz et al. 1995; Chen et al. 1995; Yuan & Narayan 2014, for review). In the BH case, the ADAF solution is a kind of radiatively inefficient accretion flow, in which a fraction of the viscously dissipated energy will be advected into the event horizon of the BH. While in the NS case, the viscously dissipated energy advected onto the surface of the NS will eventually be radiated out, so the ADAF solution is radiatively efficient (Narayan & Yi 1995b). Qiao & Liu (2018b) calculated the structure and the corresponding emergent spectrum of the ADAF around a weakly magnetized NS within the framework of the self-similar solution of the ADAF. The authors compared the electron temperature of the ADAF around a NS and a BH, it is found that the electron temperature of the ADAF around a NS is systemically lower than that of a BH, which is consistent with observations (Burke et al. 2017; Qiao & Liu 2018b). Meanwhile, the authors compared the Compton y-parameter (defined as $y = \frac{4kT_{\rm e}}{m_{\rm e}c^2}{\rm Max}(\tau_{\rm es}, \tau_{\rm es}^2)$, with $T_{\rm e}$ being the election temperature, $m_{\rm e}$ being the electron mass, c being the speed of light, and $\tau_{\rm es}$ being

★ E-mail: qiaoel@nao.cas.cn

© 2019 The Authors

the Compton scattering optical depth) of the ADAF around a NS and a BH, it is found that the Compton y-parameter of the ADAF around a NS is systemically lower than that of a BH, producing a softer X-ray spectrum, which is also consistent with observations (Wijnands et al. 2015; Parikh et al. 2017; Sonbas et al. 2018; Qiao & Liu 2018b).

Observationally, an empirical correlation between the radio luminosity and the X-ray luminosity has been established in the low/hard state of several BH-LMXBs with a form of $L_{\rm R} \propto L_{\rm X}^{\sim 0.5-0.7}$ in the range of the X-ray luminosity from $\sim 10^{32}$ to $\sim 10^{38}$ erg s^{-1}, which is generally called the 'universal' correlation (e.g. Hannikainen et al. 1998; Corbel et al. 2000, 2003; Gallo et al. 2003; Corbel et al. 2008, 2013). We should be careful that a significant deviation from the 'universal' radio/X-ray correlation is observed for some sources (such as GX 339-4) in some single outburst or decay in the X-ray luminosity range of ~ 1 order of magnitude (Corbel et al. 2013). Yuan & Cui (2005) interpreted the radio/X-ray correlation of $L_{\rm R} \propto L_{\rm X}^{\sim 0.5-0.7}$ with the radiatively inefficient accretion flow, i.e., ADAF, + jet model, in which the X-ray emission is dominated by the ADAF and the radio emission is dominated by the jet. Recently, a growing number of sources have been discovered to tend to cluster below the 'universal' correlation with a steeper correlation of $L_{\rm R} \propto L_{\rm X}^{0.98\pm0.08}$, which is possibly indicative of two distinct tracks (Gallo et al. 2012). The study for BH-LMXB H1743-322 shows that there is a correlation of $L_{\rm R} \propto L_{\rm X}^{\sim 1.4}$ in the X-ray luminosity range from $\sim 10^{36} - 10^{38}$ erg s^{-1}, and H1743-322 transits to the 'universal' correlation as it fades towards the quiescence (Coriat et al. 2011). It is suggested that the correlation of $L_{\rm R} \propto L_{\rm X}^{\sim 1.4}$ may be resulted by the transition of the accretion flow from the radiatively inefficient accretion flow, ADAF, to the radiatively efficient accretion flow, disc-corona system, with increasing the mass accretion rate (Coriat et al. 2011; Gallo et al. 2012, for discussions), which is later quantitatively interpreted by several authors with the disc-corona + jet model (e.g. Qiao & Liu 2015; Huang et al. 2014; Meyer-Hofmeister & Meyer 2014). However, we note that the statistical significance of the aforementioned two tracks, i.e., the 'universal' correlation and the steeper correlation is still questioned (Gallo et al. 2014, 2018).

For NS-LMXBs, so far, individually, the radio/X-ray correlation has been reasonably well-established only in three sources in the X-ray luminosity range of $\sim 10^{36} - 10^{37}$ erg s^{-1} , i.e., 4U 1728-34 (Migliari et al. 2003), Aql X-1 (Tudose et al. 2009; Miller-Jones et al. 2010), and EXO 1745-248 (Tetarenko et al. 2016). By fitting the data (including both the high/soft state and the low/hard state) of 4U 1728-34 with 12 simultaneous Very Large Array (VLA) and *Rossi X-ray Timing Explorer* (RXTE) observations between 2000 and 2001, it is found that the radio/X-ray correlation of 4U 1728-34 is $L_{\rm R} \propto L_{\rm X}^{\sim 1.4}$, which is consistent with what is expected by the radiatively efficient accretion flow due to the existence of the surface of the NS (Migliari et al. 2003). The fitting result for the radio/X-ray correlation of Aql X-1 is $L_{\rm R} \propto L_{\rm X}^{\sim 0.4}$, which is closer to the prediction by the radiatively inefficient accretion flow (Tudose et al. 2009). However, we should keep in mind that the data used in Tudose et al. (2009) also include the data of both the high/soft state and the low/hard state as Migliari et al. (2003). Migliari & Fender (2006) jointly fitted the data of 4U 1728-34 and Aql X-1 only in the low/hard state, the authors found that the radio/X-ray correlation is $L_{\rm R} \propto L_{\rm X}^{\sim 1.4}$ (only two points for Aql X-1 are included). Tetarenko et al. (2016) analyzed the near-simultaneous data of VLA, Australia Telescope Compact Array (ATCA), and *Swift* X-ray Telescope in the low/hard state of EXO 1745-248, located in the globular cluster Terzan 5, it is found that the radio/X-ray correlation of EXO 1745-248 is $L_{\rm R} \propto L_{\rm X}^{\sim 1.68}$.

In this paper, we focus on the radio/X-ray correlation in the low/hard state of the three NS-LMXBs 4U 1728-34, Aql X-1 and EXO 1745-248. Specifically, we collect the simultaneous radio (8.5 GHz) and X-ray (2-10 keV) data of 4U 1728-34 (Migliari et al. 2003), Aql X-1 (Migliari & Fender 2006; Tudose et al. 2009; Miller-Jones et al. 2010), and EXO 1745-248 (Tetarenko et al. 2016) in the low/hard state from literatures. We show that there is a correlation of $L_{\rm R} \propto L_{\rm X}^{1.4}$ for 4U 1728-34, a correlation of $L_{\rm R} \propto L_{\rm X}^{0.4}$ for Aql X-1, and a correlation of $L_{\rm R} \propto L_{\rm X}^{1.6}$ for EXO 1745-248 (note: the slope β here is 1.6, which is little different from the value of 1.68 in Tetarenko et al. (2016). Please refer to Section 3.3 for the reason). Then we modelled the radio/X-ray correlation of 4U 1728-34, Aql X-1 and EXO 1745-248 within the framework of the coupled ADAF-jet model respectively. We follow Qiao & Liu (2018b) for calculating the structure and the emergent spectrum of the ADAF around a weakly magnetized NS. In the coupled ADAF-jet model, we define a parameter, η, connecting the ADAF and the jet. Specifically, $\eta \equiv \dot{M}_{\rm jet}/\dot{M}$, (with $\dot{M}$ being the mass accretion rate in the ADAF and $\dot{M}_{\rm jet}$ being the mass rate in the jet), is defined to describe the fraction of the mass accretion rate in the ADAF transfered vertically forming the jet. We calculate the emission of the jet as assumed in the internal shock scenario (e.g. Yuan et al. 2005). We calculate the emergent spectrum of the coupled ADAF-jet model for $L_{\rm X}$ and $L_{\rm R}$ at different $\dot{m}$ (with $\dot{m} = \dot{M}/\dot{M}_{\rm Edd}$, and $\dot{M}_{\rm Edd} = 1.39 \times 10^{18} M/M_{\odot}$ g s^{-1}), adjusting the value of η to fit the radio/X-ray correlation of 4U 1728-34, Aql X-1 and EXO 1745-248 respectively. Then we derive a fitting formula between η and $\dot{m}$ for 4U 1728-34, Aql X-1 and EXO 1745-248 respectively. Such a relation between η and $\dot{m}$ may provide some clues on the formation mechanism and power of the jet in NS-LMXBs. Finally, we extrapolate the relation between η and $\dot{m}$ down to a lower value of $\dot{m}$, predicting a new value of X-ray luminosity and radio luminosity, which we expect could be confirmed by the observations in the future. The paper is organised as follows. The coupled ADAF-jet model is briefly introduced and discussed in Section 2. The results are shown in Section 3. The discussions are in Section 4 and conclusions are in Section 5.

2 THE MODEL

2.1 The ADAF around a weakly magnetized NS

We follow the paper of Qiao & Liu (2018b) for the structure and the emergent spectrum of the ADAF around a weakly magnetized NS. The self-similar solution of the ADAF is adopted in Qiao & Liu (2018b) as first proposed by Narayan & Yi (1995b). Specifically, we consider that the internal energy stored in the ADAF and the radial kinetic energy of the ADAF are transfered onto the surface of the NS. It is assumed that a fraction, $f_{\rm th}$, of this energy is thermalized at the surface of the NS as the soft photons to be scattered in the ADAF. We self-consistently calculate the structure of the emergent spectrum of the ADAF by considering the radiative coupling between the soft photons from the surface of the NS and ADAF itself. The structure and the corresponding emergent spectrum of the ADAF can be calculated by specifying the mass of the NS m ($m = M/M_{\odot}$), the mass accretion rate $\dot{m}$, the radius of the NS R_{*} (i.e., the inner boundary of the ADAF), the viscosity parameter α, the magnetic parameter $\beta^{'}$ (with magnetic pressure $p_{\rm m} = B^2/8\pi = (1-\beta^{'})p_{\rm tot}$, $p_{\rm tot} = p_{\rm gas} + p_{\rm m}$), and $f_{\rm th}$. As

we can see the analyses in Qiao & Liu (2018b) and Narayan & Yi (1995b), there is a critical mass accretion rate $\dot{M}_{\rm crit}$, above which the ADAF solution cannot exist. For accreting NS, the critical mass accretion rate is $\dot{M}_{\rm crit} \sim 0.1\alpha^2\dot{M}_{\rm Edd}$. Assuming a typical NS mass of $m = 1.4$, the corresponding critical luminosity is $L_{\rm crit} \sim 0.1\alpha^2 L_{\rm Edd} \sim 0.1\alpha^2 \times 10^{38}$ erg s^{-1} (with $L_{\rm Edd} = 1.26 \times 10^{38} m$ erg s^{-1} and assuming that the radiative efficiency of the ADAF is 0.1). In order to match the observed upper limits of the X-ray luminosity in the hard state (approaching or exceeding 10^{37} erg s^{-1}) of 4U 1728-34, Aql X-1 and EXO 1745-248 for the radio/X-ray correlation, we have to choose a bigger value of α. Throughout the paper, we set $\alpha = 1$ as suggest by Narayan (1996) for the luminous hard state of BH X-ray binaries. The ADAF solution often has a relatively weak magnetic field, as suggested by magnetohydrodynamic simulations (Yuan & Narayan 2014, for review). Throughout the paper, we set $\beta' = 0.95$ (Qiao et al. 2013; Qiao & Liu 2018a). Meanwhile, it is unclear how the energy of the accretion flow transfered onto the surface of the NS will interact with the NS, we simply assume $f_{\rm th} = 1$ throughout the paper, meaning that all the energy advected onto the surface of the NS is thermalized as the soft photons to be scattered in the ADAF. So, we have three free parameters left, i.e., the NS mass m, the NS radius R_*, and the mass accretion rate $\dot{m}$.

2.2 The coupled ADAF-jet model

The emission of the jet is calculated as assumed in the internal shock scenario, which has been widely used to interpret the radio emission in radio-loud quasars (Spada et al. 2001), in low-luminosity active galactic nuclei (e.g. Yu et al. 2011; Nemmen et al. 2014; van Oers et al. 2017), in the Galactic center Sgr A* (Yuan et al. 2002; Ressler et al. 2017), in the low/hard state of BH-LMXBs (Yuan et al. 2005; Zhang et al. 2010; Xie & Yuan 2016), and in gamma-ray burst (GRB) afterglow (e.g. Piran 1999) etc. In the internal shock scenario, the jet emission can be calculated by specifying the parameters as follows. (1) the mass rate $\dot{M}_{\rm jet}$ in the jet. (2) the half-opening angle of the jet ϕ (assuming the jet with a conical geometry). (3) the bulk Lorentz factor of the jet $\Gamma_{\rm jet}$. (4) $\epsilon_{\rm e}$ and $\epsilon_{\rm B}$ describing the fraction of the internal energy of the internal shock stored in the accelerated electrons and the magnetic field respectively. (5) the index, $p_{\rm jet}$, describing the power-law distribution of the electrons in the jet after the acceleration by the shock. One can refer to the detailed description for the emission of the internal shock in the Appendix of Yuan et al. (2005).

In the coupled ADAF-jet model, the accretion flow ADAF and the jet are connected by a defined parameter, $\eta \equiv \dot{M}_{\rm jet}/\dot{M}$, and $\dot{M}_{\rm jet}$ is input by assuming a value of, η, which is free parameter in the present model. The half-opening angle ϕ of the jet in the low/hard state of NS-LMXBs is uncertain. In this paper, we fix $\phi = 0.1$ as assumed by several other authors for modeling the SED of the BH-LMXBs (e.g. Yuan et al. 2005; Zhang et al. 2010). Observationally, the bulk Lorentz factor of the jet in the low/hard state of X-ray binaries can be restricted in a relatively narrow range and the velocity of the jet is mildly relativistic, i.e., $\Gamma_{\rm jet} \lesssim 2$. More strictly, the bulk Lorentz factor is restricted to be as $\Gamma_{\rm jet} \lesssim 1.67$ (Gallo et al. 2003), and $\Gamma_{\rm jet} \lesssim 1.2$ (Fender 2006). In the internal shock model, the energy density of the internal shock increases with increasing $\Gamma_{\rm jet}$, which finally will result in an increase of both the radio emission and the X-ray emission (Yuan et al. 2005). However, since $\Gamma_{\rm jet}$ is restricted in a very narrow range by observations, we expect that a slight change of $\Gamma_{\rm jet}$ will result in a slight change of the jet emission. In the present paper, we fix $\Gamma_{\rm jet} = 1.2$ corresponding the bulk velocity of the jet $\sim 0.55c$ (Fender 2006). The value of $\epsilon_{\rm e}$ and $\epsilon_{\rm B}$ describing the fraction of the internal energy of the internal shock stored in the accelerated electrons and the magnetic field, and the index, $p_{\rm jet}$, describing the power-law distribution of the electrons in the jet after the acceleration by the shock are uncertain. Qiao & Liu (2015) tested the effect of $\epsilon_{\rm e}$ and $\epsilon_{\rm B}$ on the emergent spectrum of the jet in an observationally inferred range of $0.01 < \epsilon_{\rm e} < 0.1$ and $0.01 < \epsilon_{\rm B} < 0.1$. It was found that a change of $\epsilon_{\rm B}$ in the range of $\sim 0.01 - 0.1$, the emergent spectrum of the jet nearly does not change (see the right panel of Fig. 3 of Qiao & Liu (2015)). A change of $\epsilon_{\rm e}$ in the range of $0.01 - 0.1$, the radio spectrum nearly does not change. However, the X-ray luminosity changes obviously by changing the value of $\epsilon_{\rm e}$ from $0.01 - 0.1$ (see the left panel of Fig. 3 of Qiao & Liu (2015)). As shown in the left panel of Fig. 2 of Qiao & Liu (2015), the X-ray emission is completely dominated by the accretion flow (corona) in the luminous X-ray state, which is also true in the present paper, i.e., the X-ray emission from the ADAF completely dominates the X-ray emission from the jet. In the present paper, we fix $\epsilon_{\rm e} = 0.04$ and $\epsilon_{\rm B} = 0.02$ respectively throughout the paper as (Qiao & Liu 2015). The value of the power-law index $p_{\rm jet}$ of the electron distribution in the jet predicted by the shock acceleration is $2 < p_{\rm jet} < 3$. By modeling the SEDs of three BH-LMXBs, the value of the power-law index $p_{\rm jet}$ of the electron distribution is constrained to be 2.1 (Zhang et al. 2010). Meanwhile, a change of $p_{\rm jet}$ in the range of $2 < p_{\rm jet} < 3$ has very minor effect on the X-ray spectrum. In the present paper, we fix the power-law index $p_{\rm jet} = 2.1$ throughout the paper.

Finally, we can calculate the emergent spectrum of the coupled ADAF-jet model around a weakly magnetized NS by specifying the NS m, the NS radius R_*, the mass accretion rate $\dot{m}$ and η.

3 THE RESULTS

3.1 4U 1728-34

We collect the simultaneous radio data and X-ray data of 4U 1728-34, Aql X-1 and EXO 1743-248 from literatures. For 4U 1728-34, we get the data from Migliari et al. (2003) and Migliari & Fender (2006), in which there are 12 times simultaneous radio at 8.5 GHz (VLA) and X-ray of 2-10 keV (RXTE) observations. In the present paper, we only select the hard state observations, so there are 7 observations left. For some sources observed with type I X-ray burst, especially the sources that showing the evidence of the photospheric radius expansion (PRE) can be used as a distance indicator (van Paradijs 1978). The distance of 4U 1728-34 is estimated to be as $d = 4.4 - 4.8$ kpc by taking the minimum peak flux of the radius expansion burst as the Eddington limits (assuming $R_* = 10$ km). The uncertainty of the distance arises from the probable range of the NS mass $m = 1.4 - 2.0$ (Galloway et al. 2003). We convert the flux to the luminosity of 4U 1728-34 by taking the distance as $d = 4.4$ kpc. One can see the blue open square in the panel (1) of Fig. 1 for the data. The best-fitting linear regression for the correlation between $L_{\rm R}$ and $L_{\rm X}$ gives,

$$\log L_{\rm R} = -22.93 + 1.42 \times \log L_{\rm X}, \quad (1)$$

which can be re-expressed as, $L_{\rm R} = 10^{-22.93} L_{\rm X}^{1.42}$. One can also refer to the blue solid line in the panel (1) of Fig. 1 for clarity.

In the present paper, we fix the mass and the radius of the NS in 4U 1728-34 as $m = 1.4$ and $R_* = 10$ km respectively. We calculate the emergent spectrum of the coupled ADAF-jet model for different $\dot{m}$, adjusting the value of η for $L_{\rm X}$ and $L_{\rm R}$ so that equation 1 can be satisfied. One can see the theoretical points, i.e., the

bigger-sized blue solid square in the panel (1) of Fig. 1 for details. The corresponding emergent spectra can be seen in the panel (2) of Fig. 1. Specifically, in the panel (2) of Fig. 1 from the top down, the mass accretion rates are $\dot{m} = 3.5 \times 10^{-2}$, $\dot{m} = 2.0 \times 10^{-2}$, $\dot{m} = 1.5 \times 10^{-2}$ and $\dot{m} = 8.0 \times 10^{-3}$ respectively, and the corresponding η are $\eta(\%) = 4.94$, $\eta(\%) = 5.03$, $\eta(\%) = 5.40$ and $\eta(\%) = 3.99$ respectively. Then a numerical formula of the best-fitting linear regression of η as a function of $\dot{m}$ is derived. The formula is as follows,

$$\log \eta(\%) = 0.92 + 0.14 \times \log \dot{m}, \tag{2}$$

which can be re-expressed as, $\eta(\%) = 8.34\dot{m}^{0.14}$. One can also refer to the blue solid line in Fig. 2 for clarity.

3.2 Aql X-1

We collect the simultaneous radio data and X-ray data of Aql X-1 from (Migliari & Fender 2006; Tudose et al. 2009; Miller-Jones et al. 2010). We also only select the observations in the hard state. The distance of Aql X-1 is estimated to be as $d = 5.2 \pm 0.7$ kpc by assuming the average peak luminosity of the PRE burst as $\sim 3.8 \times 10^{38}$ erg s^{-1}, or $\sim 2.0 \times 10^{38}$ erg s^{-1} (Kuulkers et al. 2003; Jonker et al. 2004). In the present paper, we convert the flux to the luminosity by assuming the distance of Aql X-1 to be as $d = 5.2$ kpc. One can see the dark green open square in the panel (1) of Fig. 1 for the data. The best-fitting linear regression for the correlation between $L_{\rm R}$ and $L_{\rm X}$ gives,

$$\log L_{\rm R} = 14.8 + 0.38 \times \log L_{\rm X}, \tag{3}$$

which can be re-expressed as, $L_{\rm R} = 10^{14.8} L_{\rm X}^{0.38}$. One can also refer to the dark green solid line in the panel (1) of Fig. 1 for clarity. In the present paper, we fix the mass and the radius of the NS in Aql X-1 as $m = 2$[1] and $R_* = 10$ km respectively. As in Section 3.1, we calculate the emergent spectrum of the coupled ADAF-jet model for different $\dot{m}$, adjusting the value of η for $L_{\rm X}$ and $L_{\rm R}$ so that equation 3 can be satisfied. The theoretical points can be seen as the bigger-sized dark green solid square in the panel (1) of Fig. 1. The corresponding emergent spectra can be seen in the panel (3) of Fig. 1. Specifically, in the panel (3) of Fig. 1 from the top down, the mass accretion rates are $\dot{m} = 2.5 \times 10^{-2}$, $\dot{m} = 1.5 \times 10^{-2}$, $\dot{m} = 1.0 \times 10^{-2}$ and $\dot{m} = 4.0 \times 10^{-3}$ respectively, and the corresponding η are $\eta(\%) = 3.25$, $\eta(\%) = 4.72$, $\eta(\%) = 6.25$ and $\eta(\%) = 11.6$ respectively. The best-fitting linear regression of η as a function of $\dot{m}$ is derived. The formula is as follows,

$$\log \eta(\%) = -0.59 - 0.69 \times \log \dot{m}, \tag{4}$$

which can be re-expressed as, $\eta(\%) = 0.26\dot{m}^{-0.69}$. One can also refer to the dark green solid line in Fig. 2 for clarity.

3.3 EXO 1745-248

EXO 1745-248 located at the globular cluster Terzan 5 is the third NS-LMXB , which has been reasonably well-established with a correlation between the radio luminosity and the X-ray luminosity (Tetarenko et al. 2016). We collect the near-simultaneous radio data and X-ray data of EXO 1745-248 in the 2015 outburst (Tetarenko et al. 2016), in which the radio data are from VLA, Australia Telescope Compact Array (ATCA), and the X-ray data are from *Swift* X-ray telescope. In the present paper, we convert the flux [2] to the luminosity by assuming the distance of EXO 1745-248 to be $d = 5.9$ kpc as that of the distance of the globular cluster Terzan 5 (Valenti et al. 2007). One can see the purple open square in the panel (1) of Fig. 1 for the data. The best-fitting linear regression for the correlation between $L_{\rm R}$ and $L_{\rm X}$ gives,

$$\log L_{\rm R} = -30.68 + 1.61 \times \log L_{\rm X}, \tag{5}$$

which can be re-expressed as, $L_{\rm R} = 10^{-30.68} L_{\rm X}^{1.61}$. One can also refer to the purple solid line in the panel (1) of Fig. 1 for clarity. As the case of Aql X-1, in the present paper, we fix the mass and the radius of the NS in EXO 1745-248 as $m = 2$ and $R_* = 10$ km respectively. Then we calculate the emergent spectrum of the coupled ADAF-jet model for different $\dot{m}$, adjusting the value of η for $L_{\rm X}$ and $L_{\rm R}$ so that equation 5 can be satisfied. One can see the bigger-sized purple solid square in the panel (1) of Fig. 1 for the theoretical points. The corresponding emergent spectra can be seen in the panel (4) of Fig. 1. Specifically, in the panel (4) of Fig. 1 from the top down, the mass accretion rates are $\dot{m} = 2.5 \times 10^{-2}$, $\dot{m} = 1.5 \times 10^{-2}$, $\dot{m} = 1.0 \times 10^{-2}$ and $\dot{m} = 6.0 \times 10^{-3}$ respectively, and the corresponding η are $\eta(\%) = 2.26$, $\eta(\%) = 2.21$, $\eta(\%) = 1.99$ and $\eta(\%) = 1.68$ respectively. The best-fitting linear regression of η as a function of $\dot{m}$ is derived. The formula is as follows,

$$\log \eta(\%) = 0.71 + 0.21 \times \log \dot{m}, \tag{6}$$

which can be re-expressed as, $\eta(\%) = 5.13\dot{m}^{0.21}$. One can also refer to the purple solid line in Fig. 2 for clarity.

As we can see from the panel (2), (3), and (4) of Fig. 1, it is clear that the radio emission is dominated by the jet, while the X-ray emission is dominated by the ADAF (energy advected on the surface of the NS) of all the three sources 4U 1728-34, Aql X-1 and EXO 1745-248.

4 DISCUSSIONS

4.1 The dependence of η on $\dot{m}$: a constraint to jet power

The relativistic jet is a very common phenomenon associated with BHs or NSs. Observationally, there are two kinds of jets in BH X-ray binaries, i.e., the compact jet and the ballistic jet. The compact jet is often associated with the low/hard state, and the ballistic jet is often associated with the spectral state transition between the low/hard state and the high/soft state (Fender et al. 2004). The compact jet is stable, and less powerful than the ballistic jet. So far, several models have been proposed for the formation mechanism of the jet around a BH, e.g., the BZ effect by Blandford & Znajek (1977) and the BP effect by Blandford & Payne (1982). In the BZ

[1] As discussed in Section 2.1, the critical luminosity of the ADAF is $L_{\rm crit} \sim 0.1\alpha^2 L_{\rm Edd} = 1.26 \times 10^{37} m$ erg s^{-1} (assuming $\alpha = 1$). Actually, for Aql X-1 and EXO 1745-248, for some points, the X-ray luminosity $L_{2-10\rm keV}$ has exceeded 10^{37} erg s^{-1}. In order to match the points with higher X-ray luminosities, we choose a bigger value of the NS mass, i.e., $m = 2$, which is often suggested to be the upper limit of the mass of the NS, to fit the radio/X-ray correlation of Aql X-1 and EXO 1745-248.

[2] In the paper of Tetarenko et al. (2016), the X-ray luminosity $L_{\rm X}$ in the range of 1-10 keV and the radio luminosity $L_{\rm R}$ at 10 GHz of EXO 1745-248 are used to measure the radio/X-ray correlation. In order to more easily to compare with the data of 4U 1728-34 and Aql X-1, we convert the X-ray luminosity $L_{\rm X}$ in the range of 1-10 keV to the range of 2-10 keV by simply assuming a photon index of $\Gamma = 1.5$, and convert the radio luminosity $L_{\rm R}$ at 10 GHz to 8.5 GHz by assuming a flat radio spectrum of $f_\nu \propto \nu^{\alpha'}$ with $\alpha' = 0$.

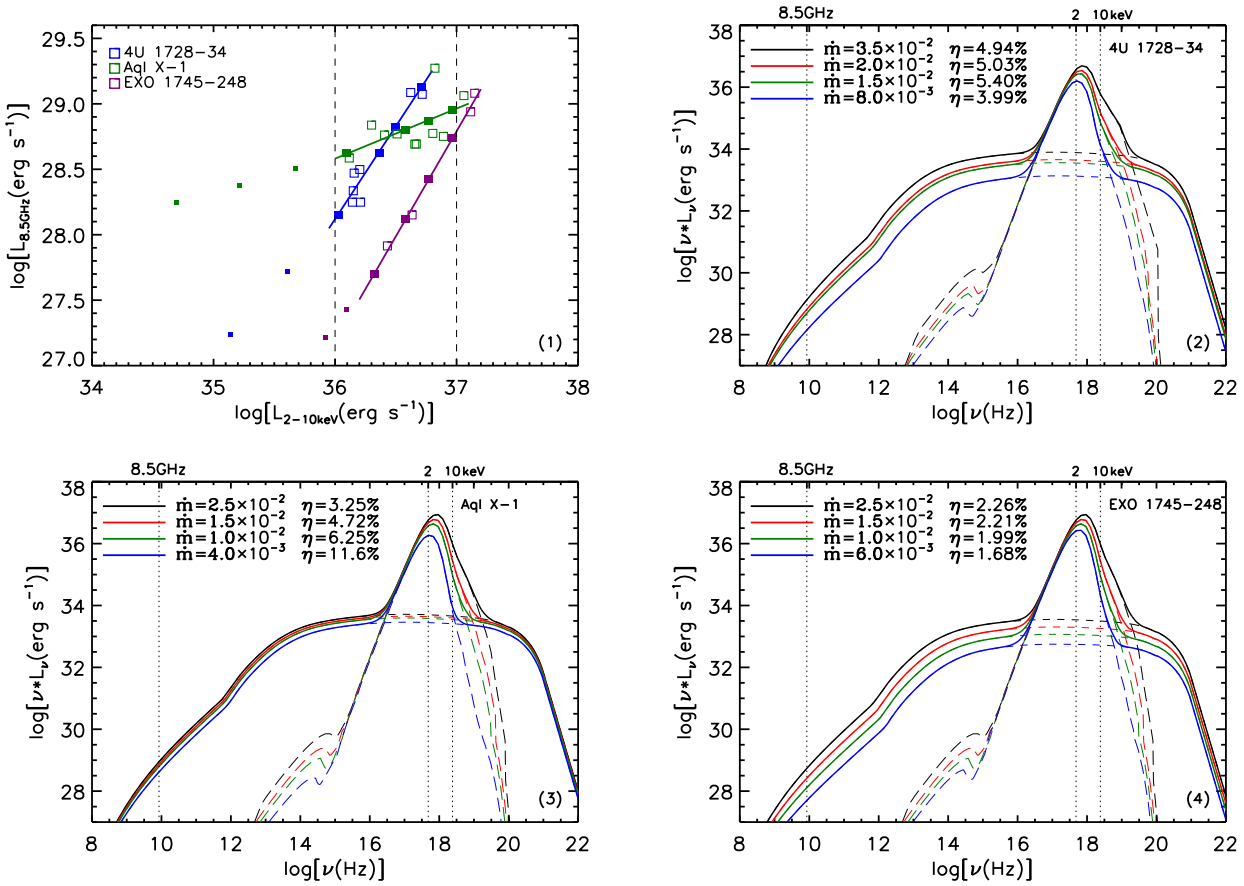


Figure 1. Panel (1): radio/X-ray correlation of 4U 1728-34, Aql X-1 and EXO 1745-248. The blue open square, the dark green open square and the purple open square are the observational data of 4U 1728-34, Aql X-1 and EXO 1745-248 respectively. The blue solid line, the dark green solid line and the purple solid line are the best-fitting linear regression for the correlation between $L_{\rm R}$ and $L_{\rm X}$ of 4U 1728-34, Aql X-1 and EXO 1745-248 respectively. The bigger-sized blue solid square, the bigger-sized dark green solid square and the bigger-sized purple solid square are the theoretical points of the coupled ADAF-jet model for fitting the radio/X-ray correlation of 4U 1728-34 (equation 1), Aql X-1 (equation 3) and EXO 1745-248 (equation 5) respectively. The smaller-sized blue solid square, the smaller-sized dark green solid square and the smaller-sized purple solid square are the theoretical points of the coupled ADAF-jet model for 4U 1728-34 (based on equation 2), Aql X-1 (based on equation 4) and EXO 1745-248 (based on equation 6) for extrapolating η as a function of $\dot{m}$ down to a lower value of $\dot{m}$ (see the text for details). Panel (2): corresponding emergent spectrum of the ADAF-jet model for 4U 1728-34. The solid line is the total emergent spectrum including the ADAF and the jet. The short-dashed line is the emergent spectrum of the jet, and the long-dashed line is the emergent spectrum of the ADAF. Panel (3): corresponding emergent spectrum of the ADAF-jet model for Aql X-1. The solid line is the total emergent spectrum including the ADAF and the jet. The short-dashed line is the emergent spectrum of the jet, and the long-dashed line is the emergent spectrum of the ADAF. Panel (4): corresponding emergent spectrum of the ADAF-jet model for EXO 1745-248. The solid line is the total emergent spectrum including the ADAF and the jet. The short-dashed line is the emergent spectrum of the jet, and the long-dashed line is the emergent spectrum of the ADAF.

effect, the jet is driven by extracting the rotational energy of the BH via a large-scale magnetic field. While in the BP effect, a large-scale magnetic field threads the accretion disc, extracting the rotational energy of the accretion disc to drive the jet. Narayan & McClintock (2012) claimed that there is a correlation between the power of the ballistic jet $P_{\rm jet}$ and the spin of the BH a_* with a form of $P_{\rm jet} \propto a_*^2$ (with $a_* = cJ/GM^2$, J being the angular momentum of the BH, G being the gravitational constant and M being the mass of the BH) by compiling a sample composed of five BH X-ray binaries with $P_{\rm jet}$ and a_* measurements (with $P_{\rm jet}$ estimated by the observed maximum radio flux at 5 GHz during the state transition, and a_* measured by the continuum-fitting method). If the claimed correlation between $P_{\rm jet}$ and a_* is true, which supports that the ballistic jet may be driven by the BZ process. However, we should also keep in mind that the claimed correlation between $P_{\rm jet}$ and a_* is still debatable, which strongly depends on how the jet power is estimated and the spin is measured. For example, Russell et al. (2013) systematically studied the dependence of the power of the ballistic jets on the spin of 12 BH X-ray binaries, the authors thought that the data do not yet support this correlation, which is still needed to be tested by the observations in the future. The origin of the compact jet in the low/hard state of BH X-ray binaries is uncertain, which is probably driven by the BP process (Fender et al. 2004, for discussions). In both BZ effect and BP effect, the power of the jet is related with the strength of the large-scale magnetic field (Livio et al. 1999).

Observationally, in the low/hard state, the power of the jet around a NS is much lower than that of a BH. Specifically, for a fixed X-ray luminosity, the radio luminosity of a NS is generally 1-2 orders of magnitude lower than that of a BH (e.g. Corbel et al. 2013; Tudor et al. 2017; Gallo et al. 2018). The study of η as function $\dot{m}$ in the present paper may provide some clues for the jet power in the low/hard state of NS. As can be seen in Section 3.1, Section

Table 1. Extrapolating value of η (based on equation 2 for 4U 1728-34, equation 4 for Aql X-1 and equation 6 for EXO 1745-248), and the corresponding X-ray luminosity L_X and the radio luminosity L_R based on the ADAF-jet model for 4U 1728-34, Aql X-1 and EXO 1745-248 respectively.

4U 1728-34			
$\dot{m}$	$\eta(\%)$	L_X(erg s^{-1})	L_R(erg s^{-1})
4×10^{-3}	3.85	4.1×10^{35}	5.2×10^{27}
2×10^{-3}	3.49	1.4×10^{35}	1.7×10^{27}
Aql X-1			
$\dot{m}$	$\eta(\%)$	L_X(erg s^{-1})	L_R(erg s^{-1})
2×10^{-3}	18.9	4.7×10^{35}	3.2×10^{28}
1×10^{-3}	30.5	1.6×10^{35}	2.4×10^{28}
5×10^{-4}	49.3	4.9×10^{34}	1.8×10^{28}
EXO 1745-248			
$\dot{m}$	$\eta(\%)$	L_X(erg s^{-1})	L_R(erg s^{-1})
4×10^{-3}	1.61	1.2×10^{36}	2.7×10^{27}
3×10^{-3}	1.51	8.4×10^{35}	1.6×10^{27}

3.2, Section 3.3, we calculate the emergent spectrum of the coupled ADAF-jet model at different $\dot{m}$, adjusting the value of η for L_X and L_R to fit the radio/X-ray correlation of 4U 1728-34, Aql X-1 and EXO 1745-248 respectively. Then, we derive a fitting formula between η and $\dot{m}$, i.e., $\eta(\%) = 8.34\dot{m}^{0.14}$, $\eta(\%) = 0.26\dot{m}^{-0.69}$, and $\eta(\%) = 5.13\dot{m}^{0.21}$ for 4U 1728-34, Aql X-1, and EXO 1745-248 respectively. One can refer to the blue solid line for 4U 1728-34, the dark green solid line for Aql X-1, and the purple solid line for EXO 1745-248 in Fig. 2 for clarity. If the derived fitting formula between η and $\dot{m}$ can be extrapolated down to a lower value of $\dot{m}$, we can predict a new value of X-ray luminosity and radio luminosity. One can see the blue dashed line, the dark green dashed line and the purple dashed line in Fig. 2 for the extrapolating part of η as a function of $\dot{m}$ for 4U 1728-34, Aql X-1 and EXO 1745-248 respectively. For 4U 1728-34, we take $\dot{m} = 4\times10^{-3}$ and $\dot{m} = 2\times10^{-3}$ as examples. The numerical results of $\eta(\%)$, and the corresponding predicted X-ray luminosity L_X and the radio luminosity L_R are shown in Table 1. One can also refer to the smaller-sized blue solid square in the panel (1) of Fig. 1 for clarity. For Aql X-1, we take $\dot{m} = 2\times10^{-3}$, $\dot{m} = 1\times10^{-3}$ and $\dot{m} = 5\times10^{-4}$ as examples. The numerical results of $\eta(\%)$, and the corresponding L_X and L_R are shown in Table 1. One can also refer to the smaller-sized dark green solid square in the panel (1) of Fig. 1 for clarity. For EXO 1745-248, we take $\dot{m} = 4\times10^{-3}$ and $\dot{m} = 3\times10^{-3}$ as examples. The numerical results of $\eta(\%)$, and the corresponding L_X and L_R are shown in Table 1. One can also refer to the smaller-sized purple solid square in the panel (1) of Fig. 1 for clarity. We expect that such the predicted X-ray luminosity and the corresponding radio luminosity for 4U 1728-34, Aql X-1 and EXO 1745-248 could be confirmed by the observations in the future.

The formation mechanism of the jet around a NS is uncertain. One of the possible mechanisms for the jet formation is the 'propeller' effect (Illarionov & Sunyaev 1975). In the 'propeller' model, when the matter in the accretion disc is accreted towards the NS, the matter is halted at the NS magnetosphere in the case of magnetic field rotating locally at super-Keplerian speed. The magnetic pressure of the magnetosphere will balance the ram pressure of the accreted matter, accelerating and ejecting a fraction of the matter in the inner region of the disc around the magnetosphere forming the jet. The 'propeller' effect works at the lower luminosity regime, and has been used to explain the emissions in the quiescent state of several Be/X-ray pulsars (Tsygankov et al. 2017). As an example, 'propeller' jet is supported by the detection of the radio emission after the fast X-ray decay during its outburst in 1998 in NS SAX J1808.4-3658 (Gaensler et al. 1999). The jet power predicted by the 'propeller' model is also uncertain, depending on the NS spin, magnetic field, accretion rate etc. (e.g. Tudor et al. 2017, for discussions). We should keep in mind that the theoretical explanation for the relatively fainter radio emission in NSs compared with that of in BHs is still a question to be answered. The studies in the present paper show that η decreases slightly with decreasing $\dot{m}$ for 4U 1728-34 and EXO 1745-248, while η increases with decreasing $\dot{m}$ for Aql X-1. One can see Fig. 2 for clarity. It is also clear that although η as a function of $\dot{m}$ has similar trends between 4U 1728-34 and EXO 1745-248, the value of η for 4U 1728-34 is roughly three times higher than that of EXO 1745-248. We note that in a wide range of $\dot{m}$, the value of η for Aql X-1 is greater than that of 4U 1728-34 and EXO 1745-248. It is very possible that the origin of the such discrepancy of η as a function of $\dot{m}$ in 4U 1728-34, EXO 1745-248 and Aql X-1 is resulted by the different strength of the large-scale magnetic field among them. Actually, a coherent millisecond X-ray pulsation (at $\sim 10^{35}$ erg s^{-1}) has been discovered in Aql X-1, while the X-ray pulsation was not discovered in 4U 1728-34 and EXO 1745-248, supporting that Aql X-1 may have a relatively stronger large-scale magnetic field compared with that of 4U 1728-34 and EXO 1745-248 for channeling the matter onto the magnetic poles (Casella et al. 2008).

4.2 The narrow X-ray luminosity range of the radio/X-ray correlation

As we can see from Section 3, for NS-LMXBs, so far, the correlation between the radio luminosity and the X-ray luminosity has been reasonably well-established only in three sources 4U 1728-34, Aql X-1 and EXO 1745-248. Meanwhile, we should keep in mind that such a radio/X-ray correlation holds only in a very narrow X-ray luminosity range ($\sim$ 1 dex) between $\sim 10^{36}$ erg s^{-1} and $\sim 10^{37}$ erg s^{-1}. As discussed in Section 4.1, currently it is unclear whether the established radio/X-ray correlation of 4U 1728-34, Aql X-1 and EXO 1745-248 in the hard state can be extended down to the X-ray luminosity regime $\lesssim 10^{36}$ erg s^{-1}. We expect that our predicted X-ray luminosity and the corresponding radio luminosity could be confirmed by the future observations. Actually, whether NS can still launch jet at lower mass accretion rates (corresponding $L_X \lesssim 10^{36}$ erg s^{-1}) is uncertain. Tudor et al. (2017) investigated the radio property and the X-ray property of three accreting millisecond X-ray pulsars (AMXPs), IGR J17511-3057, SAX J1808.4-3658 and IGR J00291+5934 during their outbursts in 2015, as well as a non-pulsing NS Cen X-4 in the low-luminosity state ($L_X \lesssim 10^{36}$ erg s^{-1}) of 2015 and the outburst in 1979. The authors found that only IGR J00291+5934 and SAX J1808.4-3658 have radio detections when they are in the low-luminosity state. Further, the authors showed that there is a complicated correlation between the radio luminosity and the X-ray luminosity in SAX J1808.4-3658 and there is a tight correlation between the radio luminosity and the X-ray luminosity in IGR J00291+5934. Recently, Gallo et al. (2018) collected a sample composed of 41 NSs with hard state Atolls and AMXPs, including three transitional millisecond pulsars (tMSPs) with the X-ray luminosity down to $\sim 10^{31}$ erg s^{-1}. Collectively, it is found that there is a correlation

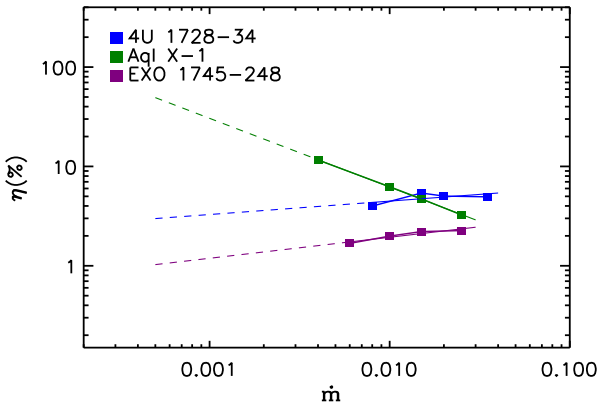


Figure 2. η as a function of $\dot{m}$. The blue solid square, the dark green solid square and the purple solid square are the theoretical points derived from the coupled ADAF-jet model for fitting the radio/X-ray correlation of 4U 1728-34 (equation 1), Aql X-1 (equation 3) and EXO 1745-248 (equation 5) respectively. The blue solid line, the dark green solid line and the purple solid line are the best-fitting linear regression between η and $\dot{m}$ of the theoretical points of 4U 1728-34, Aql X-1 and EXO 1745-248 respectively. The blue dashed line, the dark green dashed line and the purple dashed line are the extrapolating part of η as a function of $\dot{m}$ down to a lower value of $\dot{m}$ for 4U 1728-34 (based on equation 2), Aql X-1 (based on equation 4) and EXO 1745-248 (based on equation 6) respectively.

between the radio luminosity and the X-ray luminosity with the slope $\beta = 0.44^{+0.05}_{-0.04}$. While separately the slope is $\beta = 0.71^{+0.11}_{-0.09}$ for hard state Atolls, $\beta = 0.27^{+0.09}_{-0.10}$ for AMXPs, $\beta = 1.16^{+0.28}_{-0.24}$ for AMXPs weighted Atolls, and $\beta = 1.39^{+0.35}_{-0.30}$ for AMXPs-tMSPs weighted Atolls respectively. In the present paper, we focus only on the individual NS-LMXBs for their radio/X-ray correlation respectively. Meanwhile, NS-LMXBs generally have a relatively lower magnetic field ($\lesssim 10^8$ G), which is consistent with the weakly magnetized ADAF model we used in the present paper. The interpretation of the radio/X-ray correlation in AMXPs and tMSPs for $L_{\rm X} \lesssim 10^{36}$ erg s^{-1} will be continued in the future work within the framework of the modified ADAF (with stronger large-scale magnetic field considered)-jet model, which exceeds the scope of the present paper.

4.3 The effect of the NS spin

In the present paper, we consider that the internal energy stored in the ADAF and the radial kinetic energy of the ADAF are transferred onto the surface of the NS as in Qiao & Liu (2018b). Meanwhile, it is assumed that all this energy, i.e., $f_{\rm th} = 1$, is thermalized at the surface of the NS, and then radiated out as the blackbody emission to be scattered in the ADAF itself. Actually, more generally, the energy transfered onto the surface of the NS should include not only the internal energy and radial kinetic energy of the ADAF but also the rotational energy of the ADAF. The rotational energy of the ADAF will be released in a very thin boundary layer between the accretion flow and the surface of the NS. In the Newtonian approximation, the rotational energy released in the boundary layer can be expressed as,

$$L_{\rm BL} = \frac{1}{2}\dot{M}\frac{GM}{R_*}k\left(1-\frac{\nu_{\rm NS}}{\nu_*}\right)^2, \quad (7)$$

where $L_{\rm BL}$ is the rotational energy released in the boundary layer, M is the mass of the NS, R_* is the radius of the NS, k is a correction factor in the range of 0-1 ($k = 1$ for the thin disc), $\nu_{\rm NS}$ is the rotational frequency (spin) of the NS, and ν_* is the rotational frequency of the ADAF at R_*. From equation 7, it is clear that $L_{\rm BL}$ is related with the spin frequency of the NS $\nu_{\rm NS}$. If we take a typical value of $k = \frac{1}{3}$, for $\nu_{\rm NS} = 0$, $L_{\rm BL} = \frac{1}{6}\dot{M}\frac{GM}{R_*}$, meaning $\frac{1}{6}$ of the gravitational energy will be released in the boundary layer. For $\nu_{\rm NS} = \nu_*$, the rotational energy released in the boundary layer is $L_{\rm BL} = 0$. The radiation from the boundary layer will also be scattered in the ADAF, changing the structure and the X-ray emission of the ADAF. Burke et al. (2018) compiled a sample composed of nine NSs (not accreting pulsars) with well determined spin frequency. By fitting the X-ray spectra, the authors found that indeed the spin frequency of the NS is correlated with some X-ray related quantities, such as the electron temperature in corona, the Compton y-parameter, and the Compton amplification factor etc. Meanwhile, as discussed in Section 4.2 for the 'propeller' effect, theoretically, the spin of NS plays a very important role in the formation and the power of the jet. The observational hint for the correlation between the spin frequency and the jet power in NSs was confirmed by Migliari et al. (2011). A more systematic study of the effects of the spin of NS on the X-ray emission from the ADAF and the radio emission from the jet (jet power) for the radio/X-ray correlation in NSs will be continued in the future work.

5 CONCLUSIONS

In this paper, we explain the radio/X-ray correlation of three NS-LMXBs, i.e., $L_{\rm R} \propto L_{\rm X}^{\sim 1.4}$ for 4U 1728-34, $L_{\rm R} \propto L_{\rm X}^{\sim 0.4}$ for Aql X-1, and $L_{\rm R} \propto L_{\rm X}^{\sim 1.6}$ for EXO 1745-248 in their hard state within the framework of the coupled ADAF-jet model respectively. By modelling the observed radio/X-ray correlation, we derive a fitting formula of η as a function of $\dot{m}$ for 4U 1728-34, Aql X-1 and EXO 1745-248 respectively. We extrapolate the dependence of η on $\dot{m}$ to a lower value of $\dot{m}$, it is found that in a wide range of $\dot{m}$, the value of η in Aql X-1 is greater than that of in 4U 1728-34 and EXO 1745-248. The relatively higher value of η in Aql X-1 compared with that of in 4U 1728-34 and EXO 1745-248 implies that Aql X-1 may have a relatively higher magnetic field, which is supported by the discovery of the coherent millisecond X-ray pulsation (at $\sim 10^{35}$ erg s^{-1}) in Aql X-1. Finally, we predict a new X-ray luminosity and radio luminosity based on the relation between η and $\dot{m}$ extrapolating down to a lower value of $\dot{m}$. We expect that the predicted X-ray luminosity and radio luminosity can be confirmed by the future observations, with which we may give some constraints to the formation mechanism and the power of the jet for 4U 1728-34, Aql X-1, and EXO 1745-248 respectively.

ACKNOWLEDGMENTS

This work is supported by the National Natural Science Foundation of China (Grants 11773037 and 11673026), the gravitational wave pilot B (Grants No. XDB23040100), and the National Program on Key Research and Development Project (Grant No. 2016YFA0400804).

REFERENCES

Abramowicz M. A., Chen X., Kato S., Lasota J.-P., Regev O., 1995, ApJ, 438, L37
Blandford R. D., Payne D. G., 1982, MNRAS, 199, 883
Blandford R. D., Znajek R. L., 1977, MNRAS, 179, 433
Burke M. J., Gilfanov M., Sunyaev R., 2017, MNRAS, 466, 194
Burke M. J., Gilfanov M., Sunyaev R., 2018, MNRAS, 474, 760
Casella P., Altamirano D., Patruno A., Wijnands R., van der Klis M., 2008, ApJ, 674, L41
Chen X., Abramowicz M. A., Lasota J.-P., Narayan R., Yi I., 1995, ApJ, 443, L61
Corbel S., Fender R. P., Tzioumis A. K., Nowak M., McIntyre V., Durouchoux P., Sood R., 2000, A&A, 359, 251
Corbel S., Nowak M. A., Fender R. P., Tzioumis A. K., Markoff S., 2003, A&A, 400, 1007
Corbel S., Koerding E., Kaaret P., 2008, MNRAS, 389, 1697
Corbel S., Coriat M., Brocksopp C., Tzioumis A. K., Fender R. P., Tomsick J. A., Buxton M. M., Bailyn C. D., 2013, MNRAS, 428, 2500
Coriat M., et al., 2011, MNRAS, 414, 677
Done C., Gierliński M., Kubota A., 2007, A&ARv, 15, 1
Fender R., 2006, Jets from X-ray binaries. pp 381–419
Fender R. P., Belloni T. M., Gallo E., 2004, MNRAS, 355, 1105
Gaensler B. M., Stappers B. W., Getts T. J., 1999, ApJ, 522, L117
Gallo E., Fender R. P., Pooley G. G., 2003, MNRAS, 344, 60
Gallo E., Miller B. P., Fender R., 2012, MNRAS, 423, 590
Gallo E., et al., 2014, MNRAS, 445, 290
Gallo E., Degenaar N., van den Eijnden J., 2018, MNRAS, 478, L132
Galloway D. K., Psaltis D., Chakrabarty D., Muno M. P., 2003, ApJ, 590, 999
Gilfanov M., 2010, in Belloni T., ed., Lecture Notes in Physics, Berlin Springer Verlag Vol. 794, Lecture Notes in Physics, Berlin Springer Verlag. p. 17 (arXiv:0909.2567), doi:10.1007/978-3-540-76937-8˙2
Gilfanov M. R., Sunyaev R. A., 2014, Physics Uspekhi, 57, 377
Hannikainen D. C., Hunstead R. W., Campbell-Wilson D., Sood R. K., 1998, A&A, 337, 460
Huang C.-Y., Wu Q., Wang D.-X., 2014, MNRAS, 440, 965
Ichimaru S., 1977, ApJ, 214, 840
Illarionov A. F., Sunyaev R. A., 1975, A&A, 39, 185
Inogamov N. A., Sunyaev R. A., 1999, Astronomy Letters, 25, 269
Jonker P. G., Galloway D. K., McClintock J. E., Buxton M., Garcia M., Murray S., 2004, MNRAS, 354, 666
Kuulkers E., den Hartog P. R., in't Zand J. J. M., Verbunt F. W. M., Harris W. E., Cocchi M., 2003, A&A, 399, 663
Livio M., Ogilvie G. I., Pringle J. E., 1999, ApJ, 512, 100
Makishima K., Maejima Y., Mitsuda K., Bradt H. V., Remillard R. A., Tuohy I. R., Hoshi R., Nakagawa M., 1986, ApJ, 308, 635
Merloni A., Fabian A. C., Ross R. R., 2000, MNRAS, 313, 193
Meyer-Hofmeister E., Meyer F., 2014, A&A, 562, A142
Migliari S., Fender R. P., 2006, MNRAS, 366, 79
Migliari S., Fender R. P., Rupen M., Jonker P. G., Klein-Wolt M., Hjellming R. M., van der Klis M., 2003, MNRAS, 342, L67
Migliari S., Miller-Jones J. C. A., Russell D. M., 2011, MNRAS, 415, 2407
Miller-Jones J. C. A., et al., 2010, ApJ, 716, L109
Mitsuda K., et al., 1984, PASJ, 36, 741
Narayan R., 1996, ApJ, 462, 136
Narayan R., McClintock J. E., 2012, MNRAS, 419, L69
Narayan R., Yi I., 1994, ApJ, 428, L13
Narayan R., Yi I., 1995a, ApJ, 444, 231
Narayan R., Yi I., 1995b, ApJ, 452, 710
Nemmen R. S., Storchi-Bergmann T., Eracleous M., 2014, MNRAS, 438, 2804
Parikh A. S., Wijnands R., Degenaar N., Altamirano D., Patruno A., Gusinskaia N. V., Hessels J. W. T., 2017, MNRAS, 468, 3979
Piran T., 1999, Phys. Rep., 314, 575
Popham R., Narayan R., 1992, ApJ, 394, 255
Popham R., Sunyaev R., 2001, ApJ, 547, 355
Qiao E., Liu B. F., 2015, MNRAS, 448, 1099
Qiao E., Liu B. F., 2018a, MNRAS, 477, 210
Qiao E., Liu B. F., 2018b, MNRAS, 481, 938
Qiao E., Liu B. F., Panessa F., Liu J. Y., 2013, ApJ, 777, 102
Rees M. J., Begelman M. C., Blandford R. D., Phinney E. S., 1982, Nature, 295, 17
Ressler S. M., Tchekhovskoy A., Quataert E., Gammie C. F., 2017, MNRAS, 467, 3604
Russell D. M., Gallo E., Fender R. P., 2013, MNRAS, 431, 405
Shakura N. I., Sunyaev R. A., 1973, A&A, 24, 337
Sonbas E., Dhuga K. S., Göğüş E., 2018, ApJ, 853, 150
Spada M., Ghisellini G., Lazzati D., Celotti A., 2001, MNRAS, 325, 1559
Tetarenko A. J., et al., 2016, MNRAS, 460, 345
Tsygankov S. S., Wijnands R., Lutovinov A. A., Degenaar N., Poutanen J., 2017, MNRAS, 470, 126
Tudor V., et al., 2017, MNRAS, 470, 324
Tudose V., Fender R. P., Linares M., Maitra D., van der Klis M., 2009, MNRAS, 400, 2111
Valenti E., Ferraro F. R., Origlia L., 2007, AJ, 133, 1287
Wijnands R., Degenaar N., Armas Padilla M., Altamirano D., Cavecchi Y., Linares M., Bahramian A., Heinke C. O., 2015, MNRAS, 454, 1371
Xie F.-G., Yuan F., 2016, MNRAS, 456, 4377
Yu Z., Yuan F., Ho L. C., 2011, ApJ, 726, 87
Yuan F., Cui W., 2005, ApJ, 629, 408
Yuan F., Narayan R., 2014, ARA&A, 52, 529
Yuan F., Markoff S., Falcke H., 2002, A&A, 383, 854
Yuan F., Cui W., Narayan R., 2005, ApJ, 620, 905
Zhang H., Yuan F., Chaty S., 2010, ApJ, 717, 929
van Oers P., Markoff S., Uttley P., McHardy I., van der Laan T., Donovan Meyer J., Connors R., 2017, MNRAS, 468, 435
van Paradijs J., 1978, Nature, 274, 650

This paper has been typeset from a TEX/LATEX file prepared by the author.